Frequency Dependent Squeezed Light in Optomechanical Systems for Future Gravitational Wave Detection

Ana K. Lam
Barnard College, New York, NY, 10027

Mentors: Sheon Chua & Pierre-Francois Cohadon
Laboratoire Kastler Brossel, CNRS, Sorbonne Université, ENS, Paris, France 75005

July 31, 2018

Abstract

Gravitational wave detection faces sensitivity limitations due to the presence of noise sources. One of these types of noise, quantum noise, limits the future sensitivity of the LIGO and Virgo gravitational wave detectors. To overcome this quantum noise limit and increase detector sensitivity, the injection of frequency dependent squeezed light must be implemented to maximize the performance of these interferometers. The optics of gravitational wave detectors are very similar to the ones present in the high precision measurement experiments at Laboratoire Kastler Brossel. At Laboratoire Kastler Brossel, a frequency dependent squeezed light source is being coupled to an optomechanical resonator to saturate measurement sensitivity in the quantum regime. In addition to the characterization of the microresonator and the alignment of the second harmonic generator cavity, this paper focuses on the proposed three mirror filter cavity to achieve frequency dependent squeezing through tunable line width.

1 Introduction

In 1916, Albert Einstein foresaw the existence of gravitational waves, based on his theory of general relativity; however, it was not until nearly 100 years later that the first directly detected ripples in the space-time curvature, namely GW150914, would confirm that prediction (Abbott et al., 2016). Gravitational waves are transverse quadrupole waves propagated by objects whose motion is not spherically or rotationally symmetric. The distortion of space-time by these objects produces these waves that travel at the speed of light and carry that distortion. Yet, the strain of these gravitational wave distortions are extremely minuscule—on the order of 10^{-21}. Despite multiple detection efforts developing since 1960s, this "zepto-order" remains an almost constant obstacle. Because of their small size, all the noise sources present—seismic, thermal, quantum, etc.—initially completely masked the possible detection of these minute signals until

2015, when the spectacular coalescence of two black holes marked the first direct gravitational wave detection. Much of the research on gravitational wave detectors such as LIGO and Virgo is concerned with reducing noise to expand the detection range and increase detection probability of these cosmic signals.

Current gravitational wave detectors are based on the Michelson interferometer, which is designed to measure changes in distance between a central beam splitter and two arm cavities with test masses at the ends (Bond et al., 2017). As seen in Fig. 1, gravitational wave detectors face a lot of noise hindrances. Various technological configurations of detectors can increase sensitivity and help overcome the noise hindrances. Currently, detector sensitivity is limited by the quantum noise in laser light. The two sources of this type of noise are quantum shot noise (QSN) and quantum radiation pressure noise (QRPN), the former of which comes from measurement uncertainty associated in photon arrival time in the photodiode at the interferometer output. The latter, QRPN, is the result from the recoil of mirrors due to amplitude fluctuations in the laser light (Chua et al., 2014). One proposed technique to decrease this noise is implementing quantum squeezed light in the detectors.

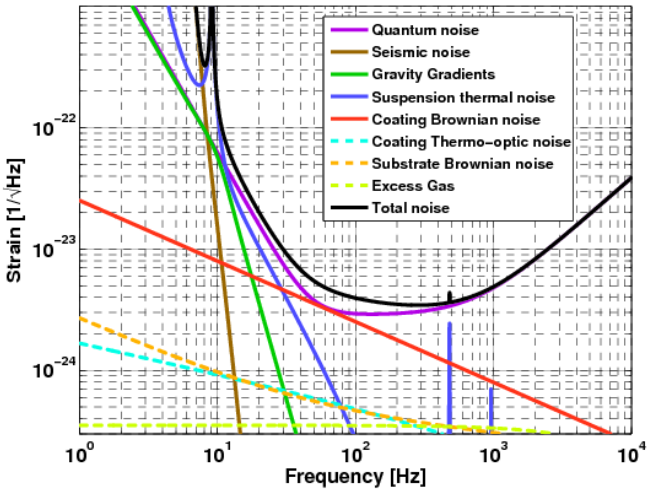

Figure 1: Advanced LIGO Design Sensitivity Curve, with expected noise limitations. Quantum noise poses a limit on the mid to high frequency range of the audio-band. Image from Hild, S.

1.1 Squeezed States of Light

Squeezed light injection is a technique used to reduce the quantum noise that is an inherent property of electromagnetic radiation. This unavoidable noise is ruled by Heisenberg's uncertainty principle which describes the fundamental uncertainty in measuring two variables (Chua et al., 2014). For laser light, the uncertainty relation for amplitude and phase quadrature is

$$\left[\hat{X}_1, \hat{X}_2\right] = 2i \tag{1}$$

$$\Delta X_1 \Delta X_2 \geqslant 1 \tag{2}$$

Now, the uncertainty principle constrains the product of error in these two variables; however, it does not necessarily constrain each variable's individual uncertainty. Therefore, there is room

for manipulation. Uncertainty in one variable can be decreased in exchange for the increase in uncertainty in the other's as long as the product still obeys Heisenberg's uncertainty principle. Here, amplitude uncertainty is squeezed by a factor of S.

$$\Delta X_1 < 1/S \qquad \Delta X_2 > S \tag{3}$$

In optics, this manipulation can be performed on phase and amplitude uncertainties of quantum states of light through nonlinear optical interactions such as those produced by nonlinear crystals (Oelker et al., 2014). Coherent states of light are often represented using a quantum phasor diagram. This diagram depicts how the quadrature uncertainty of a coherent state can be squeezed but still retain the same area of uncertainty. When the noise of the phase quadrature, ΔX_2, is decreased, the noise of the amplitude quadrature, ΔX_1, increases in response as in Fig. 2. One can choose which quadrature to "squeeze" but there is always a tradeoff.

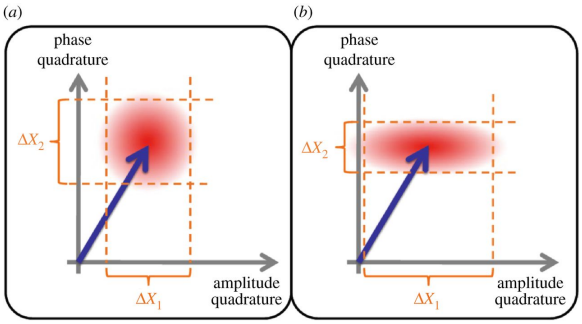

Figure 2: Phasor representation of (a) a coherent state and (b) a phase-squeezed state with proportional increase in uncertainty in the amplitude quadrature. Image from Hild, S.

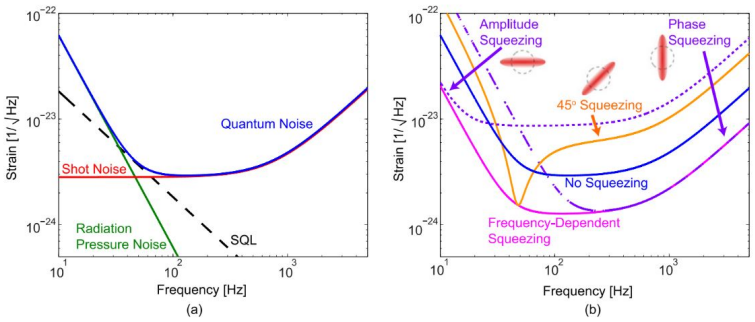

Figure 3: Gravitational wave detector (a) quantum noise curve. Shot noise limits higher frequencies and radiation pressure noise dominates the lower frequency regime. Expected sensitivity increase (b) if optimal frequency dependent squeezing is applied to gravitational wave detectors. Image from Chua, S. et al.

Vacuum fluctuations prove a hindrance to gravitational wave detectors. LIGO has already started implementing the injection of squeezed states to improve the performance of their detectors sensitivity. Using squeezed light, LIGO was able to reduce quantum shot noise which dominates in the higher frequency region of the gravitational wave frequency band. This reduced quantum noise at frequencies above 200 Hz by a significant amount (Aasi et al., 2013). Despite

the initial success of this project, it did not tackle the limit of radiation pressure noise in the lower frequency region as it was not a concern since the detectors did not have the sensitivity to encounter QRPN in the lower frequency range at that time. The two types of quantum noise have a greater effect in different regions of the gravitational wave frequency band. Thus, it is naturally ideal to introduce frequency dependent squeezed light to avoid degrading sensitivity in any frequency region. Rotating the squeezing ellipse around the standard quantum limit (SQL) can maximize sensitivity in the quantum noise limit as in Fig. 3. Depicted below are the SQL of two experiments of interest.

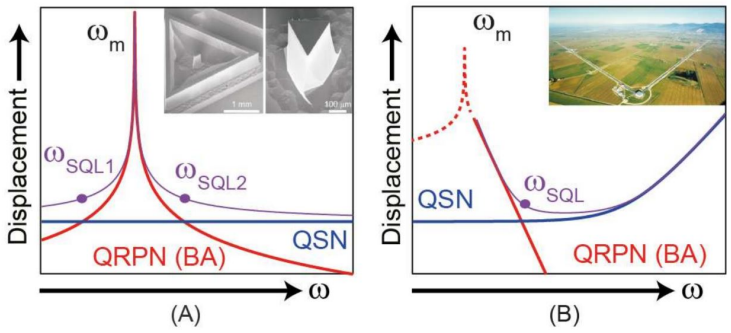

Figure 4: Quantum limit for (A) the resonant mode of the micropillar resonator and the quantum limit for (B) Virgo gravitational wave detector. Image from Chua, S. et al.

To achieve frequency dependent squeezed light, the current most developed method is a filter cavity. To achieve ideal rotation of the squeezing ellipse, the line width, or full-width-at-half-maximum (FWHM), of a signal has to match the SQL of the signal. When these are the same, the desired rotation is achieved. Fig. 5 depicts the squeezing rotation which occurs due to the phase dispersion of the cavity.

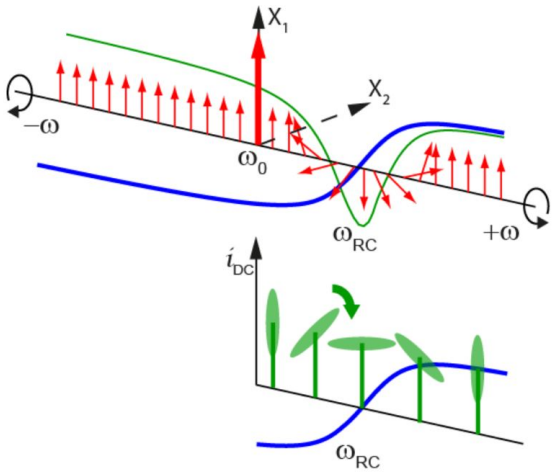

Figure 5: In the upper plot, carrier sidebands undergo 180° rotation at the maximum reflection intensity point and critical phase change point. The lower plot shows the squeezing ellipse rotation with respect to phase change. At the inflection point of the gradient there is a 90° phase change. Ideally, the point of rotation would occur at the same point of the SQLs. Image from Chua, S.

1.2 Frequency Dependent Squeezed Light for a Micromechanical Resonator

The Optomechanics and Quantum Measurement group at Laboratoire Kastler Brossel conducts experiments involving the optical processes synonymous to those in gravitational wave detectors. The micropillar experiment at Laboratoire Kastler Brossel aims at incorporating squeezed light techniques to decrease the quantum noise of a macroscopic mechanical oscillator. Thermal noise is lowered by enveloping the mechanical oscillator and the optical cavity within a cryogenic environment for the possibility of quantum state observation. Injection of squeezed light states will be needed then to decrease the quantum noise associated with radiation-pressure effects of the interface between the laser light and the quartz micropillar mechanical oscillator (Kuhn et al., 2014). This gives way for measurement sensitivity improvement beyond quantum limits, which can later be carried over to gravitational wave detector design.

1.3 Project

The squeezing experiment itself at Laboratoire Kastler Brossel involves three components: a frequency independent squeezing source, a filter cavity, and the optomechanical system. Through second order nonlinear interactions at the SHG and the OPO, a squeezed light state is yielded (Chua et al., 2014). However, this does not produce frequency dependent squeezed light. Therefore, the introduction of a unique three mirror filter cavity to this system can produce effective frequency dependent squeezing where the squeezed quadrature changes based on desired application. After this development, the frequency dependent squeezed light source will then be coupled to the optomechanics and quantum measurement experiment, as seen in Fig. 6. Despite the high precision experiment's current use of a quartz micropillar resonator, another candidate for quantum level measurements is the wheel resonator. The wheel resonator is a "low-deformation mirror" micro-oscillator made out of silicon, a material which has a highly developed manufacturing history. With the introduction of this resonator to the experiment, a characterization of its properties is needed.

The project examined the viability of a three mirror cavity with tunable reflectivity for the frequency dependent squeezed light source, review the alignment of the SHG cavity, and characterize the wheel resonator for the high precision optomechanics experiment.

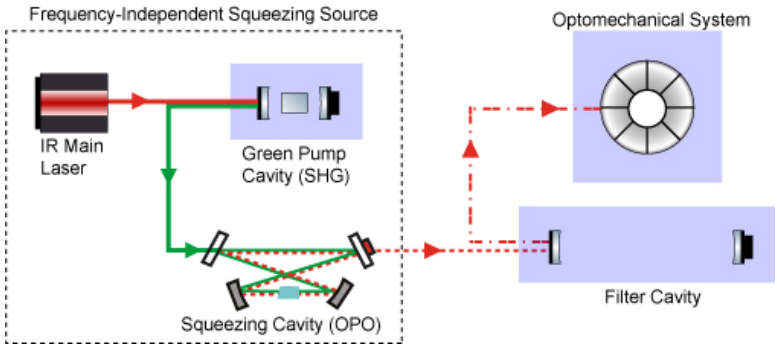

Figure 6: Overview of the squeezing and optomechanics experimental set up. The light blue shaded parts include the components of the experiment focused on in this project. Image from Chua, S. et al.

2 Three Mirror Filter Cavity

To achieve ideal frequency dependent squeezing, half the full-width-at-half-maximum of the filter cavity must be the same as the standard quantum limit Fourier frequency (in the case for gravitational wave interferometers). However, the SQL Fourier frequency is dependent on different experimental factors that can change. Therefore, a filter cavity that can tune its FWHM would be ideal to follow the changes in SQL Fourier frequency. The FWHM of a cavity signal in conjunction with free spectral range (spacing of adjacent resonance) gives the finesse of a optical system, which characterizes as the Q factor does to a mechanical system. Eq. 4, describes FWHM as a relationship of free spectral range, FSR, and finesse, $\mathcal{F}$. In addition, in Eq. 4, FWHM is given as a function of the reflectivities of the cavity mirrors, r_1 and r_2, cavity length, L, and the speed of light, c.

$$FWHM = \frac{FSR}{\mathcal{F}} \qquad FWHM = \frac{c}{2L}\frac{(1 - r_1 r_2)}{\pi r_1 r_2} \tag{4}$$

Changing mirrors every time to adjust FWHM is not efficient. A cavity with tunable reflectivities is necessary. We can devise a cavity system with this ability by replacing the front mirror of a Fabry-Perot cavity with an additional cavity. This introduced cavity can adjust its reflectivity by changing cavity length. Since this two mirror front cavity has a total reflection and transmission amplitude it is not unlike a singular mirror component which similarly has its own reflection and transmission amplitude. Hence, the first cavity acts as a "mirror" with adjustable reflectivity. With this, the FWHM of the whole three mirror system can be adjusted by simply changing the length of the first cavity which changes the reflectivity of the first "mirror." The FWHM can be tuned to match SQL Fourier frequencies and achieve optimal frequency dependent squeezing for different systems.

2.1 Two Mirror Cavity Formalism

A cavity to induce frequency dependent squeezing would follow the design based on a Fabry-Perot resonator. Traditionally, a Fabry-Perot resonator is a linear optical cavity with two reflective mirrors.

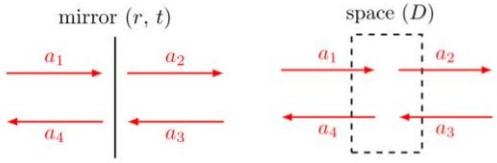

Figure 7: Coupling field amplitudes at mirror and space components. Image from Bond, C. et al.

To observe the Lorentzian curves of the signal resonance condition in the cavity, field amplitude are necessary for the transmission and reflection of the system. To derive these coefficients for such a system, one can use transfer matrices (Bond et al., 2017). For the field amplitudes

at a mirror as in Fig. 7, the transfer matrix is as follows, where r and t each represent the amplitude reflectivities and amplitude transmittances respectively.

$$\begin{pmatrix} a_1 \\ a_4 \end{pmatrix} = \frac{i}{t} \begin{pmatrix} -1 & r \\ -r & r^2 + t^2 \end{pmatrix} \begin{pmatrix} a_2 \\ a_3 \end{pmatrix} \tag{5}$$

Field amplitudes in free space, as within a cavity and as seen in Fig 6, are described by the following transfer matrix. Here, D describes the length of the free space in which the field propagates and k describes the wavenumber of the field.

$$\begin{pmatrix} a_1 \\ a_4 \end{pmatrix} = \begin{pmatrix} e^{ikD} & 0 \\ 0 & e^{-ikD} \end{pmatrix} \begin{pmatrix} a_2 \\ a_3 \end{pmatrix} \tag{6}$$

With these matrices the transfer matrix for a Fabry-Perot cavity can be computed. This matrix describing the system, in Eq. 7 and Eq. 8, contains the reflection and transmission field amplitudes of the first mirror, r_1 and t_1, and the reflection and transmission field amplitudes of the back mirror, r_2 and t_2, along with the free space within the cavity.

$$M_{cav} = M_{mirror} \times M_{space} \times M_{mirror} \tag{7}$$

$$= \frac{-1}{t_1 t_2} \begin{pmatrix} e^{ikD} - r_1 r_2 e^{-ikD} & -r_2 e^{ikD} + r_1 e^{-ikD} \\ -r_2 e^{-ikD} + r_1 e^{ikD} & e^{-ikD} - r_1 r_2 e^{ikD} \end{pmatrix} \tag{8}$$

2.2 Design of Three Mirror Cavity

The preliminary step in testing the viability of a three mirror filter cavity is in approximating a design for such a cavity. Fig. 8 depicts the three mirror cavity design examined.

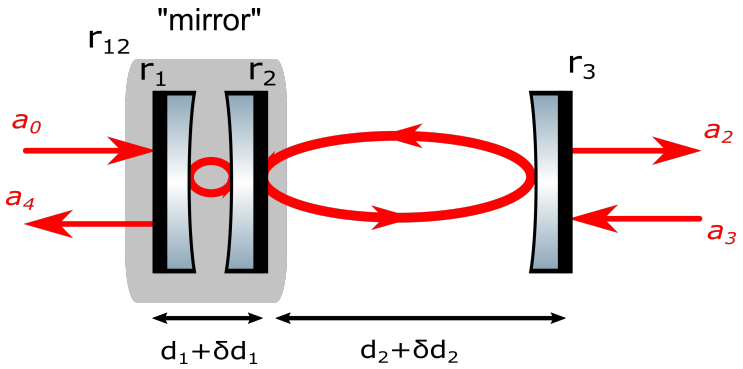

Figure 8: Three mirror cavity design. The cavity of mirror r_1 and mirror r_2 acts as one effective "mirror" with a collective reflectivity of r_{12}. Created using gwoptics component library.

Now, with the formalism of optical system matrices in Section 2.1, amplitudes for the transmission and reflection of a three mirror cavity were derived. A transfer matrix can be computed with the understanding of the components definitions and subsequently the transmission amplitude coefficient (Eq. 9) and the reflection amplitude coefficient (Eq. 10) from that and the

scattering matrix.

$$\frac{a_2}{a_0} = \frac{e^{id_1k+id_2k}t_1t_2t_3}{(1-e^{2id_1k}r_1r_2)(1-e^{2id_2k}r_3(r_1+\frac{e^{2id_1k}r_2t_1^2}{1-e^{2id_1k}r_1r_2}))} \tag{9}$$

$$\frac{a_4}{a_0} = r_1 + \frac{e^{2id_1k}r_2t_1^2}{1-e^{2id_1k}r_1r_2} + \frac{e^{(2id_1k+2id_2k)}r_3t_1^2t_2^2}{(1-e^{2id_1k}r_1r_2)^2(1-e^{2id_2k}r_3(r_1+\frac{e^{2id_1k}r_2t_1^2}{1-e^{2id_1k}r_1r_2}))} \tag{10}$$

2.3 Results

With this three mirror cavity design, it is imperative to know if the first two mirrors do indeed act as one "mirror." The length, d_1, was scanned and examined for reflection amplitudes. As seen in Fig. 9, changing the length of the first cavity "mirror" affected the reflection amplitude. This confirms that the reflectivity of the first cavity "mirror" can be manipulated by changing the its length. Now that it is confirmed that the first cavity acts as its own "mirror," verification of the three mirror cavity's performance can be done.

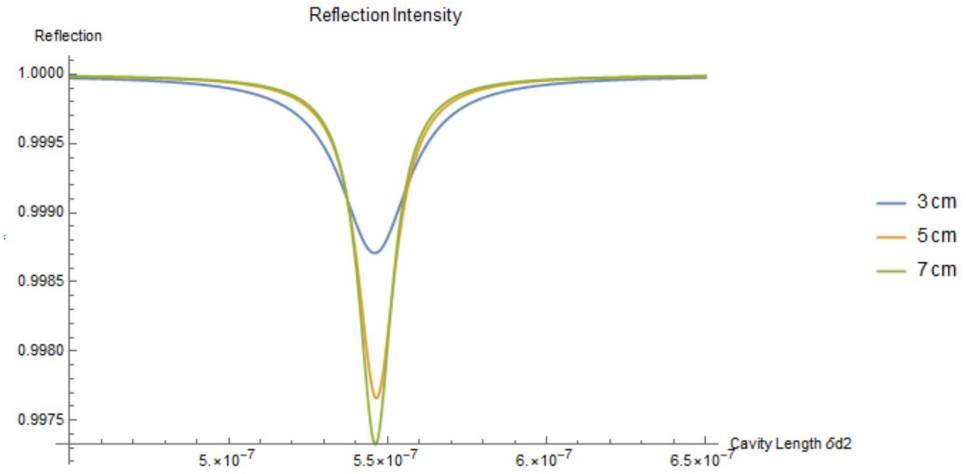

Figure 9: Reflection intensity of front "mirror" with varying d_1 lengths.

An important component in obtaining frequency dependent squeezing is achieving FWHM values that match SQL positions of signals. These FWHM values essentially affect the positions of the rotation of the squeezing ellipse. To examine the design of the cavity in response to desired FWHM values, five FWHM values that spanned over the regime of gravitational wave detectors to optomechanical experiments like the micropillar experiment were selected—100 Hz, 1000 Hz, 10000 Hz, 50000 Hz, 100000 Hz. The cavity length was set so that the first two mirror cavity was at 10 cm and the second two mirror cavity was at 1 meter with room for tuning. The total length of 1.1 meters is practical to the squeezing set up at Laboratoire Kastler Brossel.

In order to obtain such narrow FWHM values, the two mirrors of the first cavity "mirror" needed high reflectivities from the outset or else the sharp narrow linewidths would never be produced by the system. In this case, with the back mirror of the system having a reflectivity of practically 1, the first "mirror" needed to have a collective reflectivity of $R = 0.999$. With the

high reflectivities in the mirrors, the only necessary variable to adjust to achieve desired FWHM values was to change the length of the first cavity, d_1. Doing this allowed the reflectivity of the first "mirror" to be adjusted and produce desired FWHM values. The different effects of each FWHM value can be observed on the reflection intensity of the three mirror cavity (Fig. 10).

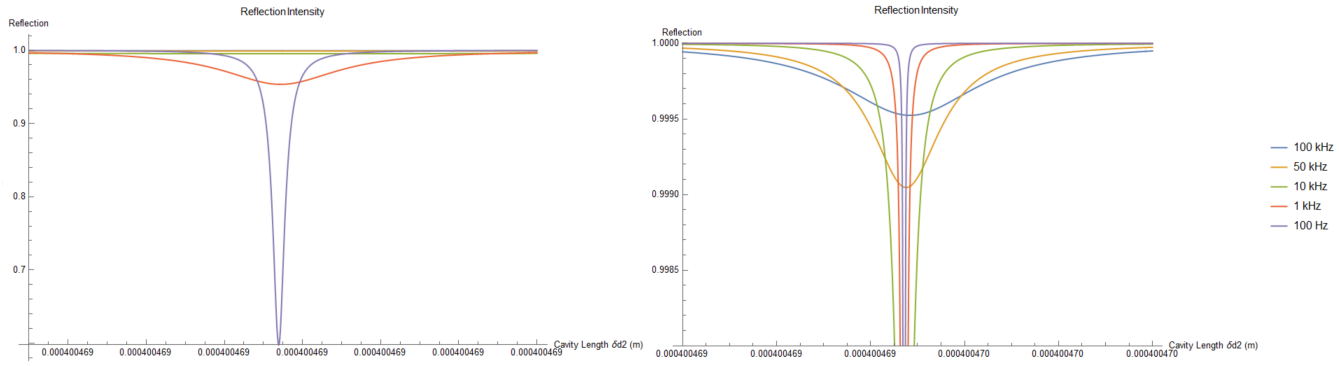

Figure 10: Reflection intensity for different full-width-at-half-maximum values (a) at a full plot range and a (b) zoomed in plot range. The zoomed in plot reveals the reflection amplitudes that are too shallow to appear in a plot that accounts for the greatest range.

The more telling plot, however, is the phase plot at different FWHM values. The phase plot indicates the rate of rotation of the squeezing ellipse. At the inflection point of the gradient, the squeezing ellipse undergoes a 90° phase change, a purely amplitude squeezed state changes into a purely phase squeezed state or vice versa. The FWHM values affect the steepness or rate of this rotation as evident in Fig. 11. This confirms that a three mirror cavity can achieve frequency dependent squeezing by changing its FWHM values to match the SQL of a desired application system.

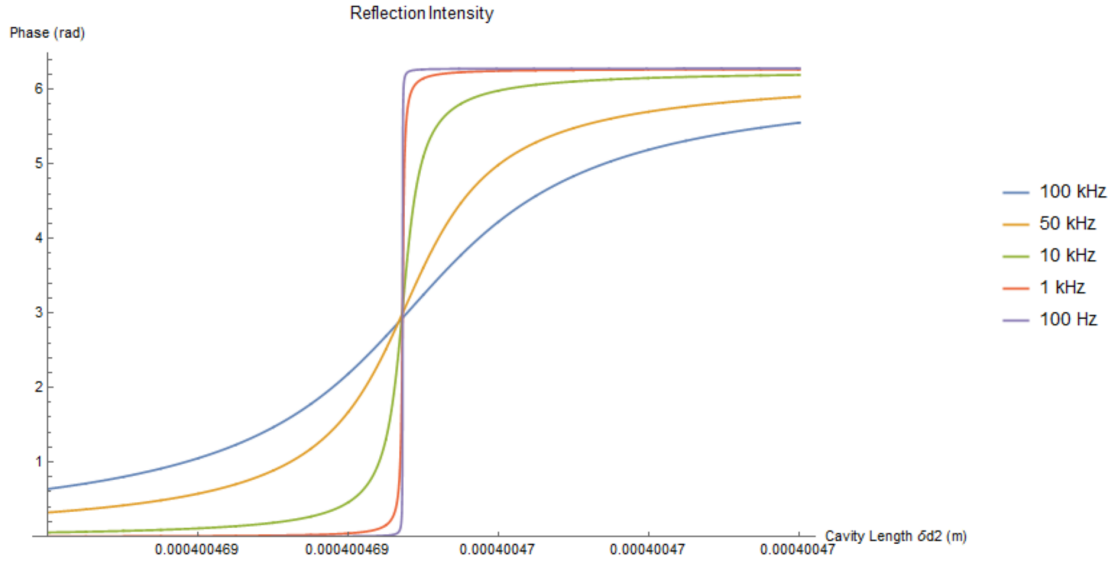

Figure 11: Phase change of signals with different full-width-at-half-maximum values. Each phase curve goes from 0 to 2π.

3 Alignment of Second Harmonic Generator Cavity

The Second Harmonic Generator (SHG) is an important component in the squeezing setup. It is where one of the nonlinear optical stages occur in the generation of squeezed light. The SHG consists of a nonlinear crystal in an oven within a Fabry-Perot cavity. At the SHG, the main laser is frequency doubled though the interaction with a nonlinear crystal which is kept at a stable temperature. In the nonlinear interaction, by the conservation of energy, the main laser is frequency doubled. This degenerate nonlinear optical process, therefore, converts 1064 nm light to 532 nm and sends it to the remaining parts of the squeezing set up, such as the Optical Parametric Oscillator (OPO).

The SHG cavity was already constructed and mounted at the time in the configuration shown in Fig 12. Yet, it was not aligned optimally. By focusing on pointing and walking the beam, the process for better alignment was conducted while observing the transmission response of the cavity in real time. Through this alignment process, the coupling to the fundamental mode of the cavity was increased while the coupling to higher order modes was minimized. This provided me with experimental experience in optics.

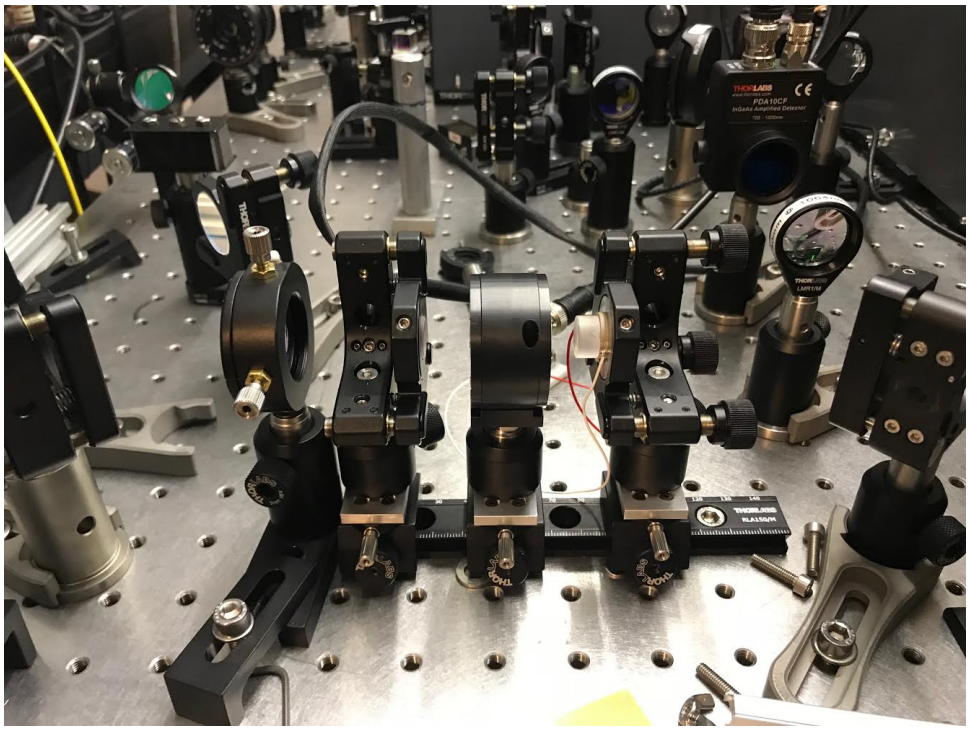

Figure 12: Second Harmonic Generator (SHG) of the squeezing experiment at Laboratoire Kastler Brossel. Its main components are the two mirrors forming a cavity and a nonlinear crystal set in an oven for temperature control.

4 Characterization of the Wheel Resonator

4.1 A "Low-Deformation" Mirror

The wheel resonator is a candidate for high precision measurement experiments in optomechanics. With its high optical finesse of 4×10^4 and high mechanical quality factor of 10^5, the micro-oscillator has ultra-low optical and mechanical losses (Serra et al., 2012). In construction, the wheel resonator is a resonator made out of thick silicon with a highly reflective mirror coating which yields high quality factors. The "low deformation" design is supported by torsional springs to avoid rotation and flexural springs for uniform vertical displacement of the mirror sans bending as seen in Fig. 13 and Fig. 14. It is a potential device to be complimentary to Laboratoire Kastler Brossel's quartz micropillar resonator because of the technological developments in silicon. Therefore an initial characterization of this device was conducted.

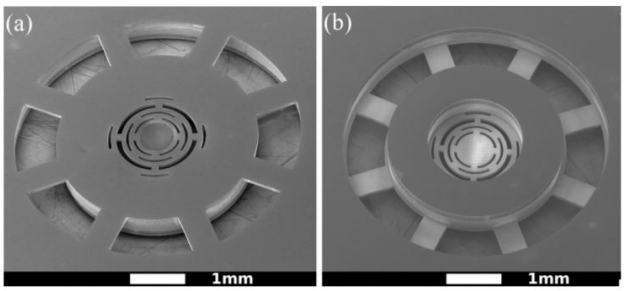

Figure 13: Scanning electron microscope image of (a) front side and (b) back side of a "low-deformation mirror" resonator made of silicon with high reflectivity coating. Image from Serra, E. et al.

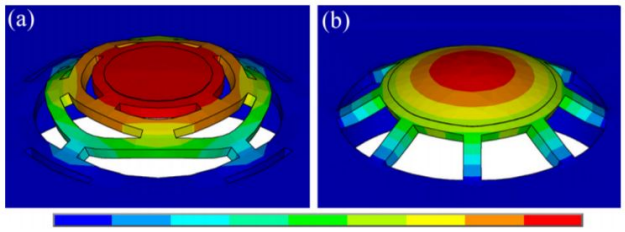

Figure 14: Modal representation of two designs. The (a) "low-deformation mirror" provides uniform displacement unlike the (b) previous design. Image from Serra, E. et al.

4.2 Results

To characterize the wheel resonator, mechanically-driven response measurements and ringdown measurements were made using a simple Michelson interferometer set up as shown in Fig. 15. To take these measurements, firstly, many alignments were needed to guarantee high fringe contrast, involving maximal fringe amplitude size, as an electrical signal scanned arm length changes with a piezo-electric actuator (PZT) in the local oscillator path. This involved aligning various lenses and both the local oscillator and wheel resonator paths by walking the beam. Then, once the Michelson interferometer was optimally aligned, the resonance frequency was recorded using a network analyzer to measure the PZT-driven displacement of the wheel resonator. This can

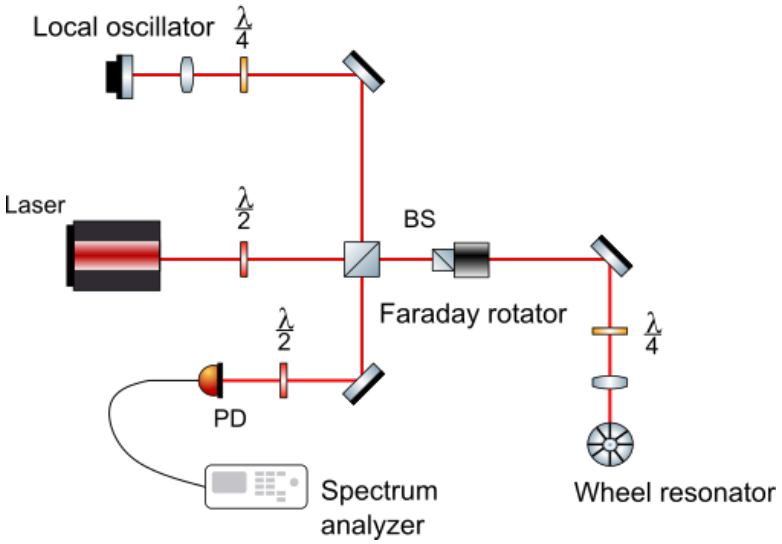

Figure 15: Set up of Michelson interferometer used for wheel resonator characterization. The wheel resonator is mounted in a vacuum chamber that can reach a temperature of approximately 2 Kelvin. Created using gwoptics component library.

both test the mechanically-driven response of the resonator and make a measurement of the mechanical resonance frequency. To retrieve the resonance frequency, a frequency sweep was induced to measure where the maximum vertical displacement occurs of the resonator's central mirror. The first mechanically-driven response measurements were taken at room temperature (300 K) and atmospheric pressure and yielded a resonance frequency of 262.084 kHz (Fig. 16).

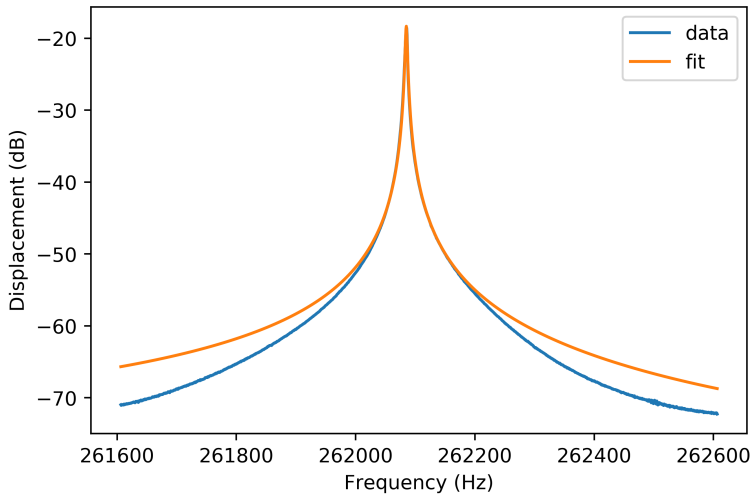

Figure 16: Frequency sweep of the mechanically-driven wheel resonator at room temperature and atmospheric pressure with a red Lorentzian fit. Peak frequency yielded was 262.084 kHz.

To measure the quality factor (Q factor) of the resonator, a ringdown measurement was performed. A ringdown measurement involves driving the resonance to a steady state and then abruptly turning off the drive and measuring the decay in vibrational energy over time. The

slope of this decay gives us the Q factor by the following relation, where a is the slope of the decay.

$$Q = \frac{f 2\pi 10 \log e}{a} \tag{11}$$

At room temperature, the Q factor measured was 7.689×10^3 (Fig. 17). This Q factor can be increased in measurements with lower temperatures and lower atmospheric temperature due to its temperature dependence.

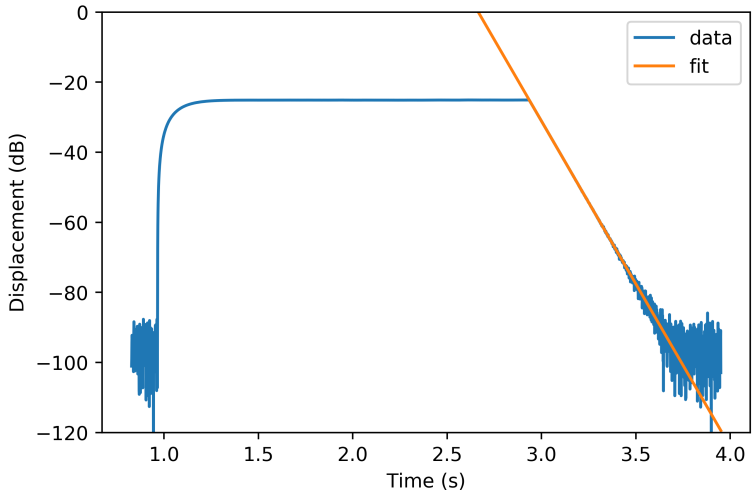

Figure 17: Ringdown measurement of the wheel resonator at room temperature and atmospheric pressure. The red linear fit yields a quality factor of 7.689×10^3.

Using the cryogenic vacuum chamber, the temperature of the sample was brought down to 6 K. Once again a ringdown measurement was taken at this temperature (Fig. 18). The drop in temperature resulted in a Q factor of 5.910×10^5.

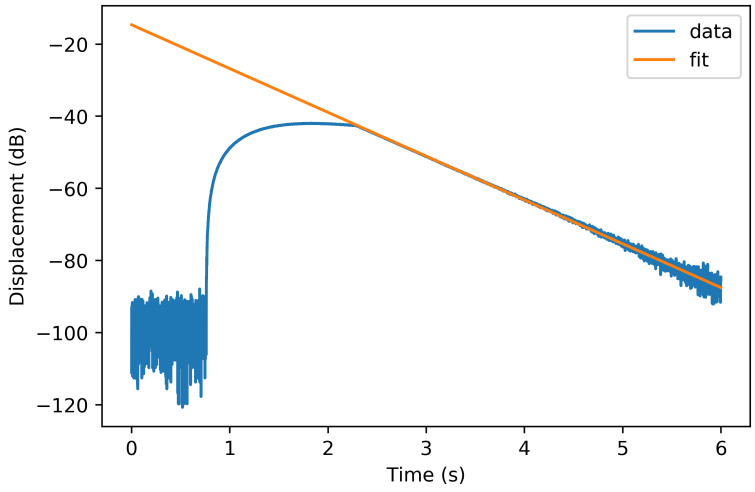

Figure 18: Ringdown measurement of the wheel resonator at 6 K. The red linear fit yields a quality factor of 5.910×10^5.

5 Conclusion

This project investigated the feasibility of a three mirror filter cavity and characterized a micro-resonator for the high precision measurement experiments at Laboratoire Kastler Brossel. From the results, it can be concluded that a three mirror filter cavity design is a feasible system to produce adjustable reflectivity and hence adjustable FWHM. This is essential for frequency dependent squeezing and therefore its production would be novel for the quantum measurement experiment at Laboratoire Kastler Brossel. The next step is to consider further features for its future implementation. For example, the investigation conducted assumed plane waves rather than Gaussian beams. In addition, a hybrid Pound-Drever-Hall technique needs to be added to this system for locking the system at desired conditions. This poses quite an obstacle for a two cavities coupled design leaving no space for locking technique for the cavity of the first two mirrors.

The initial characterization of the wheel resonator yielded reasonable data. Yet, as with most experiments, many more trials of the resonance frequency and Q factor measurements must be conducted to get robust results for the wheel resonator before its use in the quantum measurement experiment. The wheel resonator already proves complimentary due to its construction out of silicon a material with a more technologically developed manufacturing history than the quartz in the original micropillar resonator.

Aligning the SHG and Michelson interferometer provided me with my first experimental experience with optics. I learned about the techniques for alignment including beam pointing and walking the beam. Aligning the SHG allowed me to examine coupling to the fundamental mode of the cavity. Optimizing the Michelson interferometer also proved important in revealing how important optimal alignment is in later measurement accuracy.

Acknowledgements

I would like to sincerely thank everyone in the Optomechanics and Quantum Measurement group at Laboratoire Kastler Brossel for welcoming me into their lab. In particular, I would like to thank Sheon Chua, Pierre-Francois Cohadon, and Remi Metzdorff for not only involving me in their projects but also imparting an immense amount of optomechanics knowledge and experimental experience. I would also like to thank Guido Mueller, Bernard Whiting, and Kristin Nichola for organizing this program and offering me this opportunity. Lastly, I would like to thank the National Science Foundation for funding this international REU program in gravitational physics.

References

J. Aasi, J. Abadie, B. P. Abbott, R. Abbott, T. D. Abbott, M. R. Abernathy, C. Adams, T. Adams, P. Addesso, R. X. Adhikari, and et al. Enhanced sensitivity of the LIGO gravitational wave detector by using squeezed states of light. *Nature Photonics*, 7:613–619, August 2013. doi: 10.1038/nphoton.2013.177.

B. P. Abbott, R. Abbott, T. D. Abbott, M. R. Abernathy, F. Acernese, K. Ackley, C. Adams, T. Adams, P. Addesso, R. X. Adhikari, and et al. Observation of Gravitational Waves from a Binary Black Hole Merger. *Physical Review Letters*, 116(6):061102, February 2016. doi: 10.1103/PhysRevLett.116.061102.

Charlotte Bond, Daniel Brown, Andreas Freise, and Kenneth A. Strain. Interferometer techniques for gravitational-wave detection. *Living Reviews in Relativity*, 19(1):3, Feb 2017. ISSN 1433-8351. doi: 10.1007/s41114-016-0002-8. URL `https://doi.org/10.1007/s41114-016-0002-8`.

S. S. Y. Chua, B. J. J. Slagmolen, D. A. Shaddock, and D. E. McClelland. Quantum squeezed light in gravitational-wave detectors. *Classical and Quantum Gravity*, 31(18):183001, 2014. URL `http://stacks.iop.org/0264-9381/31/i=18/a=183001`.

S. Hild. Beyond the second generation of laser-interferometric gravitational wave observatories. *Classical and Quantum Gravity*, 29(12):124006, June 2012. doi: 10.1088/0264-9381/29/12/124006.

Aurlien Kuhn, Leonhard Neuhaus, Emmanuel Van Brackel, Claude Chartier, Olivier Ducloux, Olivier Le Traon, Christophe Michel, Laurent Pinard, Raffaele Flaminio, Samuel Delglise, Tristan Briant, Pierre-Franois Cohadon, and Antoine Heidmann. A micropillar for cavity optomechanics. *AIP Conference Proceedings*, 1633(1):68–70, 2014. doi: 10.1063/1.4903097. URL `https://aip.scitation.org/doi/abs/10.1063/1.4903097`.

E. Oelker, L. Barsotti, S. Dwyer, D. Sigg, and N. Mavalvala. Squeezed light for advanced gravitational wave detectors and beyond. *Opt. Express*, 22(17):21106–21121, Aug 2014. doi: 10.1364/OE.22.021106. URL `http://www.opticsexpress.org/abstract.cfm?URI=oe-22-17-21106`.

E. Serra, A. Borrielli, F. S. Cataliotti, F. Marin, F. Marino, A. Pontin, G. A. Prodi, and M. Bonaldi. A low-deformation mirror micro-oscillator with ultra-low optical and mechanical losses. *Applied Physics Letters*, 101(7):071101, 2012. doi: 10.1063/1.4745510. URL `https://doi.org/10.1063/1.4745510`.

Appendix

A Mathematica Code Extract

In[268]:=
```
(*THREE MIRROR CAVITY*)
```

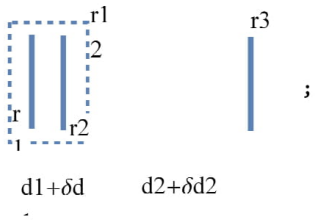

In[34]:=
```
(*CONFRIMATION/CHECK OF R IN SECOND CAVITY*)
rFP[r1_, r2_, t1_, t2_, d1_] =
  (t1^2 * r2 * Exp[I * 2 * k * d1] / (1 - r1 * r2 * Exp[I * 2 * k * d1]) + r1);
tFP[r1_, r2_, t1_, t2_, d1_] = t2 * t1 * Exp[I * k * d1] / (1 - r1 * r2 * Exp[I * 2 * d1 * k]);
```

In[36]:=
```
rtwo = rFP[r12, r3, t12, t3, d2];
ttwo = tFP[r12, r3, t12, t3, d2];
partwo = {t12 → I * Sqrt[1 - r12^2], t3 → I * Sqrt[1 - r3^2], r3 → Sqrt[1 - ϵ], r12 → R / r3,
   ϵ → 0.000001, k → (2 * π) / (λ + δλ), λ → 1064 * 10^(-9), d2 → 1, δλ → dλ / 1064 * 10^(-9)};
```

In[39]:=
```
(*Different reflectivies*)
refl100k = {R → 0.997906};
refl50k = {R → 0.998953};
refl10k = {R → 0.999790};
refl1k = {R → 0.999979};
refl100 = {R → 0.999998};
```

In[50]:=
```
(*FWHM CALCULATION*)
```

In[51]:=
```
(*100kHz*)
FindMinimum[Abs[rtwo //. partwo //. refl100k], {dλ, 0.149}]
```

In[52]:=
```
{0.9995229448427712`, {dλ → 0.14943668854762765`}};
```

In[53]:=
```
1 - ((1 - 0.999523) / 2)
```

In[54]:=
```
0.9997615` (*FWHM y-value*)
```

In[55]:=
```
With[{f = Abs[rtwo //. partwo //. refl100k] &},
   Reap@Plot[f@dλ, {dλ, 0.1492, 0.1493}, EvaluationMonitor :→ Sow@{dλ, f@dλ}]][[2, 1]];
```

In[56]:=
```
With[{f = Abs[rtwo //. partwo //. refl100k] &}, Reap@
    Plot[f@dλ, {dλ, 0.149233, 0.14926}, EvaluationMonitor :→ Sow@{dλ, f@dλ}]][[2, 1]];
```

In[57]:=
```
dif = 0.14963729059140188` - 0.14923741349481495`;
```

In[58]:=
```
(*Difference between two end points of FWHM*)
FWHM = ((dif * (1064*^-9)) * (c / ((1064*^-9)))) / L

119880.13768369792` (*Check, close to 100kHz*)
```

In[105]:=
```
(*For R=0.999790, x=0.0004006401287993624`*)
```

In[106]:=
```
(*1kHz*)
With[{f = Abs[rtwo2 //. partwo2] &},
   Reap@Plot[f@δd1, {δd1, 4.00649 * 10^(-4), 4.006493 * 10^(-4)},
     EvaluationMonitor :> Sow@{δd1, f@δd1}]][[2, 1]];
```

In[107]:=
```
(*For R=0.999979, x=0.0004006490852692032*)
```

In[108]:=
```
(*100Hz*)
With[{f = Abs[rtwo2 //. partwo2] &},
   Reap@Plot[f@δd1, {δd1, 4.00675 * 10^(-4), 4.0069 * 10^(-4)},
     EvaluationMonitor :> Sow@{δd1, f@δd1}]][[2, 1]];
```

In[109]:=
```
(*For R=0.999998, x=0.00040067896850339057`*)
```

In[110]:=

In[111]:=
```
(*FINDING 5 FWHM's FOR THREE MIRRORS*)
```

In[112]:=
```
rfirstcavity = rFP[r1, r2, t1, t2, d1];
tfirstcavity = tFP[r1, r2, t1, t2, d1];
rthree = rFP[rfirstcavity, r3, tfirstcavity, t3, d2]
```

Out[114]=
$$r1 + \frac{e^{2\,i\,d1\,k}\,r2\,t1^2}{1 - e^{2\,i\,d1\,k}\,r1\,r2} + \frac{e^{2\,i\,d1\,k+2\,i\,d2\,k}\,r3\,t1^2\,t2^2}{\left(1 - e^{2\,i\,d1\,k}\,r1\,r2\right)^2\left(1 - e^{2\,i\,d2\,k}\,r3\left(r1 + \frac{e^{2\,i\,d1\,k}\,r2\,t1^2}{1 - e^{2\,i\,d1\,k}\,r1\,r2}\right)\right)}$$

In[115]:=
```
parthree = {t1 → I * Sqrt[1 - r1^2], t2 → I * Sqrt[1 - r2^2],
   t3 → I * Sqrt[1 - r3^2], R → 0.999, r1 → Sqrt[R], r2 → Sqrt[R], r3 → Sqrt[1 - ϵ],
   ϵ → 0.000001, k → (2 * π) / (λ), λ → 1064*^-9, d1 → 0.1 + δd1, d2 → 1 + δd2};

d100k = {δd1 → 0.00040063730605545596`};
d50k = {δd1 → 0.0004006378490043906`};
d10k = {δd1 → 0.0004006401287993624`};
d1k = {δd1 → 0.0004006490852692032};
d100 = {δd1 → 0.00040067896850339057`};
```

In[129]:=
```
(*FWHM Calculation*)

(*100kHz*)
FindMinimum[Abs[rthree //. parthree //. d100k], {δd2, 0.0004004695}]
```

In[130]:=
```
{0.9995261370472479`, {δd2 → 0.00040046947139004823`}};
```

In[131]:=
```
(1 - (1 - 0.9995261370472479`) / 2)
```

In[132]:=
```
0.999763068523624`; (*FWHM y-value*)
```

In[133]:=
```
With[{f = Abs[rthree //. parthree //. d100k] &}, Reap@Plot[f@δd2,
     {δd2, 0.0004004693, 0.00040046931}, EvaluationMonitor :> Sow@{δd2, f@δd2}]][[2, 1]];
```

```
In[134]:= With[{f = Abs[rthree //. parthree //. d100k] &}, Reap@Plot[f@δd2,
            {δd2, 0.00040046965, 0.00040046967}, EvaluationMonitor :> Sow@{δd2, f@δd2}]][[2, 1]];

In[135]:= dif = 0.00040046966306324556` - 0.00040046930490043956`

In[136]:= FWHM = (dif) * (c / ((1064*^-9))) / (1 + .1)

In[137]:= 91741.71904892112` (*FWHM*)

In[138]:=
          (*50kHz*)

In[139]:= FindMinimum[Abs[rthree //. parthree //. d50k], {δd2, 0.0004004679}]

In[140]:= {0.9990489163944053`, {δd2 → 0.0004004678720340084`}};

In[141]:= (1 - (1 - 0.9990489163944053`) / 2)

In[142]:= 0.9995244581972027`; (*FWHM y-value*)

In[143]:= With[{f = Abs[rthree //. parthree //. d50k] &}, Reap@Plot[f@δd2,
            {δd2, 0.00040046777, 0.00040046779}, EvaluationMonitor :> Sow@{δd2, f@δd2}]][[2, 1]];

In[144]:= With[{f = Abs[rthree //. parthree //. d50k] &}, Reap@Plot[f@δd2,
            {δd2, 0.00040046796, 0.00040046799}, EvaluationMonitor :> Sow@{δd2, f@δd2}]][[2, 1]];

In[145]:= dif = 0.00040046796549103635` - 0.00040046778714371657`;

In[146]:= FWHM = (dif) * (c / ((1064*^-9))) / (1 + .1)

In[147]:= 45682.82756949508` (*FWHM*)


In[148]:= (*10kHz*)

In[149]:= FindMinimum[Abs[rthree //. parthree //. d10k], {δd2, 0.00040046575}]

In[150]:= {0.9952647273981916`, {δd2 → 0.00040046573609251216`}};

In[151]:= (1 - (1 - 0.9952647273981916`) / 2)

In[152]:= 0.9976323636990958`;(*FWHM y-value*)

In[153]:= With[{f = Abs[rthree //. parthree //. d10k] &},
            Reap@Plot[f@δd2, {δd2, 0.0004004657187, 0.000400465719},
              EvaluationMonitor :> Sow@{δd2, f@δd2}]][[2, 1]];

In[154]:= With[{f = Abs[rthree //. parthree //. d10k] &},
            Reap@Plot[f@δd2, {δd2, 0.0004004657544, 0.0004004657548},
              EvaluationMonitor :> Sow@{δd2, f@δd2}]][[2, 1]];

In[155]:= dif = 0.00040046575450582710` - 0.00040046571877304756`;
          FWHM = (dif) * (c / ((1064*^-9))) / (1 + .1)

In[157]:= 9152.783497904578` (*FWHM*)
```